Available online at www.sciencedirect.com

ScienceDirect

Publishing Services by Elsevier

International Journal of Naval Architecture and Ocean Engineering 10 (2018) 170–179
http://www.journals.elsevier.com/international-journal-of-naval-architecture-and-ocean-engineering/

A study of hydroelastic behavior of hinged VLFS

Yonggang Sun [b,d], Da Lu [d], Jin Xu [a,b], Xiantao Zhang [c,*]

[a] PLA University of Science and Technology, Nanjing, PR China
[b] Wuxi First Scientific Research Institute, Wuxi, PR China
[c] Center for Offshore Foundation Systems, School of Civil, Environmental and Mining Engineering, University of Western Australia, Australia
[d] State Key Laboratory of Ocean Engineering, Shanghai Jiao Tong University, Shanghai, PR China

Received 1 January 2017; revised 28 March 2017; accepted 9 May 2017
Available online 7 August 2017

Abstract

This paper introduces a new method to study the hydroelastic behavior of hinged Very Large Floating Structures (VLFSs). A hinged two-module structure is used to confirm the present approach. For each module, the hydroelasticity theory proposed by Lu et al. (2016) is adopted to consider the coupled effects of wave dynamics and structural deformation. The continuous condition at the connection position between two adjacent modules is also satisfied. Then the hydroelastic motion equation can be established and numerically solved to obtain the vertical displacement, force and bending moment of the hinged structure. The results calculated by the present new method are compared with those obtained using three-dimensional hydroelasticity theory (Fu et al., 2007), which shows rather good agreement.

Keywords: Hydroelasticity; VLFS; Hinged structures; Frequency domain; Multi-body

1. Introduction

Very Large Floating Structures (VLFSs) are very flexible offshore structures which are widely regarded as an alternative option of ocean space utilization. Due to their obvious advantages including environmental friendliness, easy and fast construction and removal and low cost in construction, VLFSs have been gradually designed for various applications such as floating airports, bridges, oil storage facilities and floating artificial island. Most VLFSs can be categorized into two types, i.e. single-module VLFS and interconnected multi-module VLFS. For these flexible floating structures, the coupling between structural deformation and fluid field becomes a significant factor when it comes to their dynamic response in waves. For single-module VLFSs, many theories have been proposed to predict their response (Wu, 1984; Tsubogo and Okada, 1998; Tuitman et al., 2012; Lu et al., 2016). Based on these theories, the dynamic response of various types of VLFSs has been investigated. Wu et al. (2014) calculated the hydrodynamic response of multi-leg floating structures. Pan et al. (2015) investigated the hydrodynamic response of mooring lines for a large floating structure in the South China Sea.

For hinged multi-module VLFSs, some researchers (Newman, 1994; Gou et al., 2004) studied their dynamic response by neglecting the elastic deformation of the structure. Fu et al. (2007) combined three-dimensional hydroelasticity theory and multi-rigid-body kinematics to consider the hydroelastic response of an articulated VLFS. In addition, the Mindlin plate element method was also used to obtain the hydrodynamic response of two articulated VLFSs (Kim et al., 2007; Gao et al., 2011). Riyansyah et al. (2010) used the Euler–Bernoulli beam to study articulated VLFSs without considering the effect of the floating body on the fluid.

The purpose of this paper is to propose a new method to calculate the hydroelastic response of interconnected multi-

* Corresponding author.
E-mail address: zhxter@outlook.com (X. Zhang).
Peer review under responsibility of Society of Naval Architects of Korea.

http://dx.doi.org/10.1016/j.ijnaoe.2017.05.002

module VLFSs. The hinge is assumed to be rigid while each module of the VLFSs is assumed to be flexible with structural deformation considered. As a simple case, the hinged two-module VLFS model adopted by Fu et al. (2007) is used here to confirm the present method. The present approach is a combination of the hydroelasticity theory for a single-module continuous VLFS proposed by Lu et al. (2016) and hinged rigid multi-body theory. For each module, the hydroelasticity theory proposed by Lu et al. (2016) is adopted to consider the coupled effects of wave dynamics and structural deformation. At the hinged position, the method of Gou (Gou et al., 2004) is used to consider the continuous condition. Then the hydroelastic motion equation can be established and numerically solved to obtain the vertical displacement, force and bending moment of the hinged structure. All results calculated by the present approach are compared with those obtained by three-dimensional hydroelasticity theory (Fu et al., 2007).

2. Basic theory

2.1. Multi-body hydroelasticity theory

As the results calculated using the present approach are compared with those obtained by three-dimensional hydroelasticity theory proposed by Fu et al. (2007), this paper will give a brief introduction of Fu's method before we move forward to a detailed description of the present approach. For simplicity, we avoid listing many mathematical equations and introduce the main idea of Fu's method (more details can refer to Fu's paper). Actually, the approach proposed by Fu et al. (2007) is classic three-dimensional hydroelasticity theory, in which the hydroelastic response of flexible floating structures can be calculated in three main steps:

(1) Evaluation of the dry natural oscillation mode for hinged two-module flexible structure.
(2) Evaluation of the hydrodynamic coefficients (added mass, radiation damping and wave excitation force) for each mode.
(3) Solving the coupling modal equation to obtain the hydroelastic response of the hinged flexible structure.

The hydroelasticity theory for a continuous flexible structure proposed by Lu et al. (2016) is adopted in this paper. Unlike traditional three-dimensional hydroelasticity theory (Fu et al., 2007), in the approach proposed by Lu et al. (2016), the coupling between structural deformation and fluid field is considered by (imaginarily) dividing the continuous structure into several submodules and adding a virtual beam between the center of each submodule. Then multi-body hydrodynamics and beam bending theory can be combined together to deal with the dynamic response of flexible structure without considering the natural mode of the dry structure. The present work actually extends Lu's theory to deal with a more complex problem, i.e. the dynamic response of (rigidly) hinged multi-module flexible structure (not a continuous structure in the Lu's work) in waves. For the integrity of the paper, we will revisit the method of Lu et al. (2016) in this section. For the hydrodynamic aspect, this paper adopts the assumption of ideal fluid, i.e., the fluid is inviscid, irrotational, and incompressible. The incident wave amplitude is assumed to be small relative to a characteristic wavelength and body dimension, and therefore linear Airy wave theory can be applied. The hydrodynamic coefficients of the equivalent multi-module floating structures considering diffraction and radiation effects can be calculated using the conventional potential theory (In this paper, the commercial software Hydrostar is used to obtain these hydrodynamic coefficients).

Fig. 1 is a schematic of hinged multi-module flexible floating structure and its surrounding fluid field. The number of modules for the floating structure is m. Two adjacent modules are hinged together. In Lu's theory, a continuous (single-module) flexible structure is divided into several submodules to approximately consider the coupled effects of wave dynamics and structural deformation (using multi-body hydrodynamics and beam theory). So for multi-module flexible structure, each module is divided into several submodules (the number of submodules for each module is n shown in Fig. 1). Based on the assumptions of an ideal fluid and linearity, the velocity potential can be decomposed into three parts as follows:

$$\phi = \phi_{\mathrm{I}} + \phi_{\mathrm{D}} + \phi_{\mathrm{R}} \tag{1}$$

where ϕ_I, ϕ_D and ϕ_R denotes, respectively, the incident wave potential, diffraction wave potential, and radiation wave potential. The incident, diffraction potential and radiation potential satisfy the following boundary conditions:

$$\begin{cases} \nabla^2\phi = 0, & in\ \Omega \\ -\omega^2\phi + g\dfrac{\partial\phi}{\partial z} = 0, & on\ S_F \\ \dfrac{\partial\phi}{\partial z} = 0, & on\ S_B \\ \dfrac{\partial(\phi_I + \phi_D)}{\partial z} = 0, & on \sum\limits_{q=1}^{m\times n} S_q \\ \dfrac{\partial\phi_{Rk}}{\partial n_k} = \overrightarrow{V}_{S_k}\cdot\overrightarrow{n}_k & on\ S_k (k = 1, 2, ..., n\times m) \\ \dfrac{\partial\phi_{Rk}}{\partial n_j} = 0 & on \sum\limits_{j=1, j\neq k}^{m\times n} S_j \\ \lim\limits_{r\to\infty}\sqrt{r}\left(\dfrac{\partial\phi_{Rk}}{\partial r} - \dfrac{i\omega^2}{g}\phi_{Rk}\right) = 0 & on\ S_\infty \end{cases} \tag{2}$$

where (see Fig. 1) Ω is the fluid domain, and S_F, S_B, and S_∞ are the free surface, bottom surface, and the boundary surface at infinity of the fluid, respectively. S_k (S_j) represents the wetted body surface of the kth (jth) submodule ($k, j = 1, 2, \ldots, n \times m$; $j \neq k$). $\overrightarrow{n}_k$ represents the outward-directed unit vector normal to the wetted surface of the kth submodule, $\overrightarrow{V}_{S_k}$ is the velocity of a given point on the wetted surface of the kth submodule,

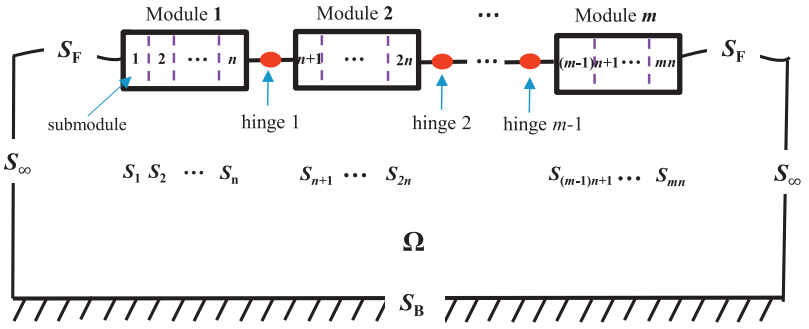

Fig. 1. Definition of the fluid and structure boundaries.

and ϕ is the velocity potential (In Eq. (2), ϕ can be replaced by ϕ_I, ϕ_D or ϕ_R). r is the distance between the far-field point and the source point. After the velocity potential ϕ is obtained, the added mass and the radiation damping of these submodules as well as the wave excitation force can be calculated.

In the frequency domain, the excitation forces are related to the incident and diffracted wave potentials as follows:

$$\overrightarrow{F}_{exk} = \rho i\omega \iint_{S_{0k}} (\phi_I + \phi_D) \cdot \overrightarrow{n}_k dS \tag{3}$$

where i, $\overrightarrow{F}_{exk}$, ρ, ω and S_{0k} are the imaginary unit, wave excitation forces, fluid density, wave frequency, and average wetted surfaces, respectively.

The added mass and radiation damping is given by

$$[a_{kj}] + \frac{i}{\omega}[b_{kj}] = \rho \iint_{S_{0k}} \phi_{Rj} \cdot \overrightarrow{n}_k dS. \tag{4}$$

where $[a_{kj}]$ is the added mass matrix of the kth submodule induced by the motion of the jth submodule, $[b_{kj}]$ is the radiation damping matrix of the kth submodule caused by the motion of the jth submodule ($k, j = 1, 2, \ldots, n \times m$).

The equation of motion of freely floating multi-body system (In Fig. 1, the multi-body system comprises $m \times n$ submodules and each submodule has a six degree-of-freedom motion) in the frequency domain for a unitary wave amplitude and a wave frequency ω is given as follows:

$$\left(-\omega^2([\mathrm{M}_k] + [a_{kk}]) - i\omega[b_{kk}] + [C_k]\right)\{u_k\} + \sum_{j=1, j\neq k}^{n\times m} \left(-\omega^2[a_{kj}] - i\omega[b_{kj}]\right)\{u_j\} = \{f_{exk}\} \quad (k = 1, 2, \ldots, n \times m) \tag{5}$$

where $[M_k]$ is the mass (or inertia moment) matrix of the kth submodule, $[a_{kk}]$is the added mass (or added mass moment) matrix of the kth submodule caused by the motion of the submodule itself, $[b_{kk}]$ is the radiation damping matrix of the kth submodule caused by the motion of the submodule itself, $[C_k]$ is the hydrostatic stiffness matrix of the kth submodule, $\{f_{exk}\}$ is the wave excitation force (or moment) of the kth submodule, and $\{u_k\}$ is the six DOF displacement of the kth submodule expressed as $(x_k, y_k, z_k, \alpha_k, \beta_k, \gamma_k)^{\mathrm{T}}$. It should be noted that in Eq. (5), the restraint of displacement due to the existence of hinge connections and the structural deformation of each submodule are not considered. The dimension is 6×6 for $[M_k]$, $[a_{kk}]$, $[b_{kk}]$, $[C_k]$, $[a_{kj}]$ and $[b_{kj}]$ and 6×1 for $\{u_k\}$ and $\{f_{exk}\}$ ($k, j = 1, 2, \ldots, n \times m$).

If the displacement restraint due to the existence of hinge connections is taken into account (for example, the hinge connection between the submodule n and $n + 1$, $2n$ and $2n + 1$, …, $(m - 1) \times n$ and $(m - 1) \times n+1$ shown in Fig. 1), Eq. (5) can be modified as follows (refer to Gou et al., 2004),

$$\left(-\omega^2([\mathrm{M}_k] + [a_{kk}]) - i\omega[b_{kk}] + [C_k]\right)\{u_k\} + \sum_{j=1, j\neq k}^{n\times m} \left(-\omega^2[a_{kj}] - i\omega[b_{kj}]\right)\{u_j\} = \{f_{exk}\} + \{F_{Lk}\} \quad (k = 1, 2, \ldots, n \times m) \tag{6}$$

where $\{F_{Lk}\}$ (the dimension is 6×1) is the force and moment acting on the floating structure caused by the connection piece, which only exists in the two connected submodules (for example, as shown in Fig. 1, $\{F_{Lk}\} \neq \{0\}$ for $k = n, n + 1, 2n, 2n + 1, \ldots, (m - 1) \times n, (m - 1) \times n + 1$. However, for k being other values, $\{F_{Lk}\} = \{0\}$). m is the number of modules for the floating system. In order to solve the equations, the

continuous condition of displacement at the connection point is needed. The translational motion of two hinged submodules is the same while the angular motion is different. Only angular motion around the y axis is allowed with a rigid horizontal hinge shaft (parallel to the y axis). The continuous displacement condition is expressed as follows:

$$[\mathrm{L}]\{u\}_{i-j} = [0 \quad 0 \quad 0 \quad 0 \quad 0]^T \tag{7}$$

In Eq. (7), $\{u\}_{i-j} = [\{u_i\}^T \{u_j\}^T]^T$(the dimension is 12×1) is the displacement of hinged submodules i and j. The restraint coefficient matrix $[L]$ is given as

$$[L] = \begin{bmatrix} 1 & 0 & 0 & 0 & z_i & -y_i & -1 & 0 & 0 & 0 & -z_j & y_j \\ 0 & 1 & 0 & -z_i & 0 & x_i & 0 & -1 & 0 & z_j & 0 & -x_j \\ 0 & 0 & 1 & y_i & -x_i & 0 & 0 & 0 & -1 & -y_j & x_j & 0 \\ 0 & 0 & 0 & 1 & 0 & 0 & 0 & 0 & 0 & -1 & 0 & 0 \\ 0 & 0 & 0 & 0 & 0 & 1 & 0 & 0 & 0 & 0 & 0 & -1 \end{bmatrix}_{5\times 12} \tag{8}$$

where, (x_i, y_i, z_i) and(x_j, y_j, z_j) are the local coordinates of the connection point in the body-fixed coordinate system of submodule i and submodule j, respectively. It should be noted that for each submodule, the local coordinate system has the origin at the center of gravity of the submodule.

We denote the force (and moment) on the pth hinge piece as $\{f_L^p\} = (f_{L1}^p, f_{L2}^p, f_{L3}^p, f_{L4}^p, f_{L5}^p)^T$, the component of which represents, respectively, the force in x, y, z direction and the moment with respect to x and z axis (as the hinge shaft is parallel to the y axis, the moment with respect to y axis is zero and is not included in the force vector). Then the force and moment acting on the $(p \times n)$th and $(p \times n + 1)$th submodule caused by the hinge piece is give as follows:

$$\begin{bmatrix} \{\mathrm{F}_L\}_{p\times n} \\ \{F_L\}_{p\times n+1} \end{bmatrix}_{12\times 1} = -[L]^T_{12\times 5}\{f_L^p\}_{5\times 1} \tag{9}$$

If we apply the method proposed by Lu et al. (2016) to each module (each module will be divided into several submodules to approximately consider the coupling effects of structural deformation and fluid field) of the hinged multi-module flexible structure, the motion of the center of a submodule is restricted by the deformation condition of the equivalent beam between two submodules. This means that the motion of the kth submodule will be affected by its adjacent submodules $(k-1)$th and $(k+1)$th in terms of structural deformation. For the first and the last (the $(m \times n)$th) submodule, the motion is only affected by the second and the $(m \times n - 1)$th submodule, respectively. Based on this analysis, Eq. (6) will be modified as follows:

$$\begin{aligned} &(-\omega^2([\mathrm{M_k}] + [a_{kk}]) - i\omega[b_{kk}] + [C_k])\{u_k\} \\ &+ \sum_{j=1, j\neq k}^{n\times m} \left(-\omega^2[a_{kj}] - i\omega[b_{kj}]\right)\{u_j\} = \{f_{exk}\} + \{F_{Lk}\} + \{F_{Sk}\} \\ &(k = 1, 2, \ldots, m \times n) \end{aligned} \tag{10}$$

where$\{F_{Sk}\}$ is the force (and moment) acting on the kth submodule caused by the structural deformation of the equivalent beam between the adjacent submodule and itself. The expression of $\{F_{Sk}\}$ will be given in Section 2.2.

By solving Eq. (10), the six DOF motion of each body and the forces on the connectors can be obtained, and then the deformation and force of the structure can be obtained using Lu's method (Lu et al., 2016).

2.2. Solution of deformation and force

In order to approximately consider the coupling between the structural deformation and fluid field, the six degree-of-freedom (DOF) motion of a submodule's center is restricted by the deformation condition of the equivalent beam between two adjacent submodules (For more details, refer to Lu et al., 2016).

Each side of the beam element $i - j$ has six components of displacements and forces (shown in Fig. 2):

$$\begin{aligned} \{u\}_{i-j} &= \left[\{u\}_i^T \{u\}_j^T\right]^T = \left[x_i, y_i, z_i, \alpha_i, \beta_i, \gamma_i, x_j, y_j, z_j, \alpha_j, \beta_j, \gamma_j\right]^T \\ \{F\}_{i-j} &= \left[\{F\}_i^T \{F\}_j^T\right]^T = \left[Fx_i, Fy_i, Fz_i, Mx_i, My_i, Mz_i, Fx_j, Fy_j, Fz_j, Mx_j, My_j, Mz_j\right]^T \end{aligned} \tag{11}$$

where (Fx_i, Fy_i, Fz_i) are forces in the ith cross section, (Mx_i, My_i, Mz_i) are the corresponding bending moments. Similar expressions can be obtained for the jth cross section. Generally, the forces and moments are assumed to be imposed on the center of the cross section of the beam element.

The relationship between $\{u\}_{i-j}$ and $\{F\}_{i-j}$ is:

$$\{F\}_{i-j} = [\mathrm{K}]_{i-j}\{u\}_{i-j} \tag{12}$$

where $[K]_{i-j}$ is stiffness matrix, the form of which is given in the Appendix. A detailed explanation of the stiffness matrix can be found in the reference (McGuire et al., 2000). The size of the matrix is 12×12. The matrix is affected by the geometric size of each submodule, Young modulus and Poisson ratio.

Next, we will give the expression of $\{F_{Sk}\}$ in Eq. (10). As shown in Fig. 3, $\{F_{Sk}\}$ is the force (and moment) acting on the kth submodule caused by the structural deformation of the equivalent beam between the adjacent submodule and itself

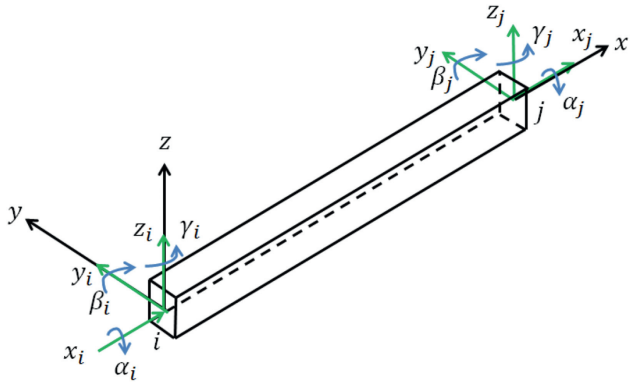

Fig. 2. The coordinate of space structure.

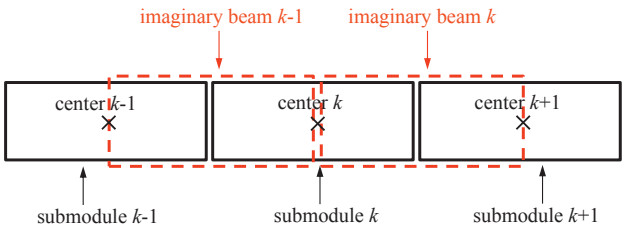

Fig. 3. A schematic of submodules and imaginary beam between adjacent submodules.

(i.e., imaginary beam $k-1$ and k). According to Eq. (12), we can establish the relationship between force and displacement for both beam $k-1$ and k, as follows,

$$\begin{bmatrix}\{F\}_{k-1}^{k-1}\\ \{F\}_{k}^{k-1}\end{bmatrix} = -\begin{bmatrix}[K]_{k-1,k-1}^{k-1} & [K]_{k-1,k}^{k-1}\\ [K]_{k,k-1}^{k-1} & [K]_{k,k}^{k-1}\end{bmatrix}\begin{bmatrix}\{u\}_{k-1}^{k-1}\\ \{u\}_{k}^{k-1}\end{bmatrix} \tag{13}$$

$$\begin{bmatrix}\{F\}_{k}^{k}\\ \{F\}_{k+1}^{k}\end{bmatrix} = -\begin{bmatrix}[K]_{k,k}^{k} & [K]_{k,k+1}^{k}\\ [K]_{k+1,k}^{k} & [K]_{k+1,k+1}^{k}\end{bmatrix}\begin{bmatrix}\{u\}_{k}^{k}\\ \{u\}_{k+1}^{k}\end{bmatrix} \tag{14}$$

where the superscript represents the order number of the beam and the subscript represents the order number of the sub-module's center. $[K]_{k-1,k-1}^{k-1}$ and $[K]_{k-1,k}^{k-1}$, etc. are the partitioned matrix of the stiffness matrix shown in the Appendix. It should be note that $\{u\}_k^{k-1} = \{u\}_k^k$. So we may neglect the superscript of the displacement matrix. Thus we have the expression $\{F_{Sk}\}$ as follows,

$$\begin{aligned}\{F_{Sk}\} &= \{F\}_k^{k-1} + \{F\}_k^k\\ &= -\begin{bmatrix}[K]_{k,k-1}^{k-1} & [K]_{k,k}^{k-1} + [K]_{k,k}^{k} & [K]_{k,k+1}^{k}\end{bmatrix}_{6\times 18}\begin{bmatrix}\{u\}_{k-1}^T & \{u\}_k^T & \{u\}_{k+1}^T\end{bmatrix}_{18\times 1}^T\end{aligned} \tag{15}$$

Lu et al. (2016) proposed an approach for the computation of the displacement along a continuous (single-module) VLFS based on the spatial beam theory. In this paper, a more generalized method will be developed.

It can be seen from Eq. (12) that once the displacement $\{u\}_{i-j}$ has been solved, the load on the section of the beam $\{F\}_{i-j}$ can be computed. For a given spatial beam, the displacement along the beam can be calculated based on the displacement and loads on the cross section at the end of the beam.

Eq. (12) can be rewritten as

$$\begin{bmatrix}\{F\}_i\\ \{F\}_j\end{bmatrix} = \begin{bmatrix}[K]_{ii} & [K]_{ij}\\ [K]_{ji} & [K]_{jj}\end{bmatrix}\begin{bmatrix}\{u\}_i\\ \{u\}_j\end{bmatrix} \tag{16}$$

The force $\{F\}_i$ and $\{F\}_j$ can be obtained once the displacement $\{u\}_i$ and $\{u\}_j$ have been solved.

In order to calculate the displacement $\{u\}_l$ and force $\{F\}_l$ at any position along the beam, Eq. (16) is modified as follows

$$\begin{bmatrix}\{F\}_i\\ \{F\}_l\end{bmatrix} = \begin{bmatrix}[K]_{ii} & [K]_{il}\\ [K]_{li} & [K]_{ll}\end{bmatrix}\begin{bmatrix}\{u\}_i\\ \{u\}_l\end{bmatrix} \tag{17}$$

Then the displacement $\{u\}_l$ and force $\{F\}_l$ can be computed by

$$\begin{cases}\{u\}_l = [K]_{il}^{-1}\left(\{F\}_i - [K]_{ii}\{u\}_i\right)\\ \{F\}_l = [K]_{li}\{u\}_i + [K]_{ll}\left\{[K]_{il}^{-1}\left(\{F\}_i - [K]_{ii}\{u\}_i\right)\right\}\end{cases} \tag{18}$$

Eq. (18) can give all the six components of displacement along the VLFS, which is a big improvement of the original method proposed by Lu et al. (2016).

In the origin work of Lu, the continuous distribution force are simplified as the concentrated force on the gravity center of the sub-module, only the connection interface of the sub-modules are exactly right. However, it can be seen from Eq. (18) that on the exact point (the connection interface of the sub-modules), both the bending moment value and its partial derivative with respect to the variable x are known. Therefore the higher order interpolation scheme can be applied. Li et al. (1986) shows that the interpolation cures can be cubic order if both the point value and its partial derivative of the two ending points are known, i.e. $\{x_i, My_i, Fz_i\}$ and$\{x_{i+1}, My_{i+1}, Fz_{i+1}\}$ are known. Here, x_i, My_i and Fz_i represents the position, bending moment and shear force, respectively, which follows the definition of symbols in Eq. (11). Then the interpolation curve can be expressed as:

$$M(x) = a + bx + cx^2 + dx^3 \tag{19}$$

where

$$\begin{bmatrix}a\\ b\\ c\\ d\end{bmatrix} = \begin{bmatrix}1 & x_i & x_i^2 & x_i^3\\ 1 & x_{i+1} & x_{i+1}^2 & x_{i+1}^3\\ 0 & 1 & 2x_i & 3x_i^2\\ 0 & 1 & 2x_{i+1} & 3x_{i+1}^2\end{bmatrix}\begin{bmatrix}My_i\\ My_{i+1}\\ Fz_i\\ Fz_{i+1}\end{bmatrix} \tag{20}$$

Since in the current method, both the bending moment and the shear force are taken into account when solving the bending moment distribution along the VLFS, then the interpolation accuracy must be higher than the original method of Lu.

3. Numerical examples

In order to validate the new method proposed in this paper, we investigated two cases in this section: one is a hinged two-module rigid structure; the other is a hinged two-module flexible structure.

3.1. A hinged two-module rigid structure

The hinged two-module rigid structure investigated by Newman (1994) is used in this test. The model comprises two identical homogeneous square modules hinged together so as to allow relative rotation around the y axis. In the calculation, the water depth is assumed to be infinite. The schematic of the two square modules is shown in Fig. 4 (the distribution of grids is $40 \times 10 \times 5$). The size of each square module is, and the draft is 5 m. The wave direction is 0°, parallel to the x axis. The grids used in the hydrodynamic calculation are also shown.

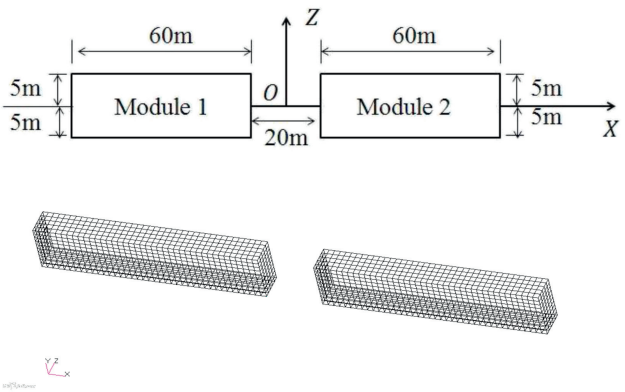

Fig. 4. Hinged model and grids used in the hydrodynamic calculation.

Based on the numerical calculation, the relative pitch angle of the two square modules and the displacement at the connection point is compared with Newman's results. Fig. 5 shows the relative pitch angle (α) of the two square modules, which is normalized by the wave steepness (KA, with K being the wave number and A the incident wave amplitude). Fig. 6 gives the normalized heave displacement of the connection point. As can be seen from Figs. 5 and 6, the results calculated by the present numerical method (using the commercial code Hydrostar) are in good agreement with the results of Newman (1994). The fluctuation shown in Figs. 5 and 6 is caused by the period of incident wave close to the natural period of the floating system (Gou et al., 2004).

3.2. A hinged two-module flexible structure

To illustrate this methodology, this paper uses the model described by Yokosuka (see the reference, Yago and Endo, 1996). This VLFS is a scale model of the Mega-Float, constructed and developed for use in sheltered waters. The main parameters of the floating system are listed in Table 1. In order to get a hinged two-module flexible structure which has the same dimension as the one described by Yokosuka, we divided the continuous model into two parts and the two modules are

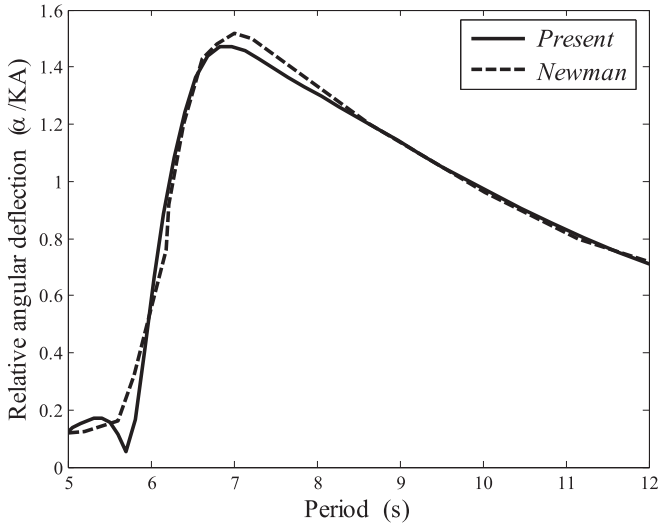

Fig. 5. Relative angular deflection.

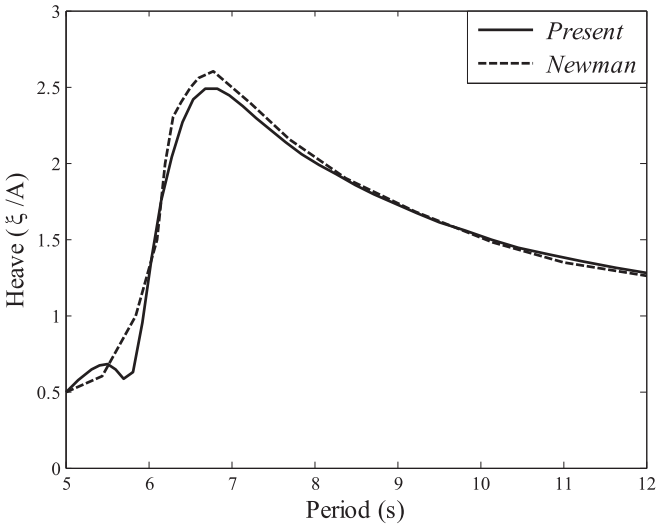

Fig. 6. Heave amplitude at the hinged joint.

Table 1
Parameters of the floating system.

Parameters	Units	Value
Length	m	300
Width	m	60
Depth	m	2
Draft	m	0.5
Young's modulus	N/m^2	1.19×10^{10}
Poisson's ratio	ν	0.13
Density	kg/m^3	256.25
Water depth	m	58.5

hinged together. The model was also adopted for hydroelasticity analysis by Fu et al. (2007). The result calculated by the method presented in this paper is compared to those of Fu.

In Fig. 7, the hinged connector are at the middle of longitudinal direction of the structure and parallel to the width direction (y axis). P_2 represents the position where the hinged shaft is located. P_1 is the center of the cross section at the left side of the structure. The waves pass from the left to the right and the amplitude is 1 m. In this calculation, each of the two modules is divided into four submodules to approximately couple the structural deformation and fluid field. So the total number of submodules for the two-module flexible structure is eight. For an illustrative purpose, this paper only calculates the case shown in Fu's paper (Fu et al., 2007).

In Fig. 8, the vertical response amplitude of the longitudinal centerline is calculated for four different wavelengths. The result for hinged two-module rigid structure is also shown. The value calculated by three-dimensional hydroelasticity theory is expressed as “Fu et al., 2007”; the result of the present method “Present”; and the result of hinged two-module rigid structure “Rigid”. It is clear that the result calculated using the present approach is in good agreement with Fu's results, but the results for rigid structure are very different (due to structure deformation being neglected). All the results show that the elasticity has great influences on the hydrodynamic response of the hinged flexible structure.

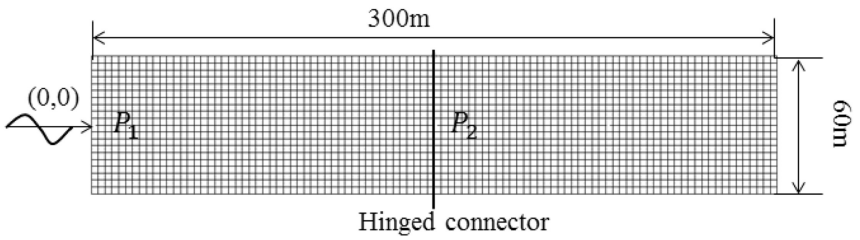

Fig. 7. Schematic plane view of a two-module, interconnected structure.

In Fig. 9, the vertical displacement of points P_1 and P_2 with respect to wave frequency are given, normalized by the wave amplitude (A). Satisfactory agreement is observed between the present approach and three-dimensional hydroelasticity theory (Fu et al., 2007). There is also a significant difference of results between flexible structure and rigid structure, which indicates the importance of structural deformation when calculating the dynamic response of hinged VLFSs.

The force on the connector was not given by Fu et al. (2007) due to the limitation of their approach. However, the new method proposed in this paper can tackle the problem (by solving Eq. (10)). The shear force F_z and F_x at the hinged point is given in Fig. 10 for both hinged two-module rigid structure and flexible structure. It is clearly seen that the force F_x is almost the same for two cases, but the peak value of the shear force F_z is very different. However, the variation of the shear force with respect to the wave frequency shows a similar trend for the rigid and elastic structure.

The structure's bending moment is obtained using Lu's method (Lu et al., 2016) and the present method, labeled as "Lu et al., 2016" and "Present" in Fig. 11. The results obtained by the present method match well with those calculated using

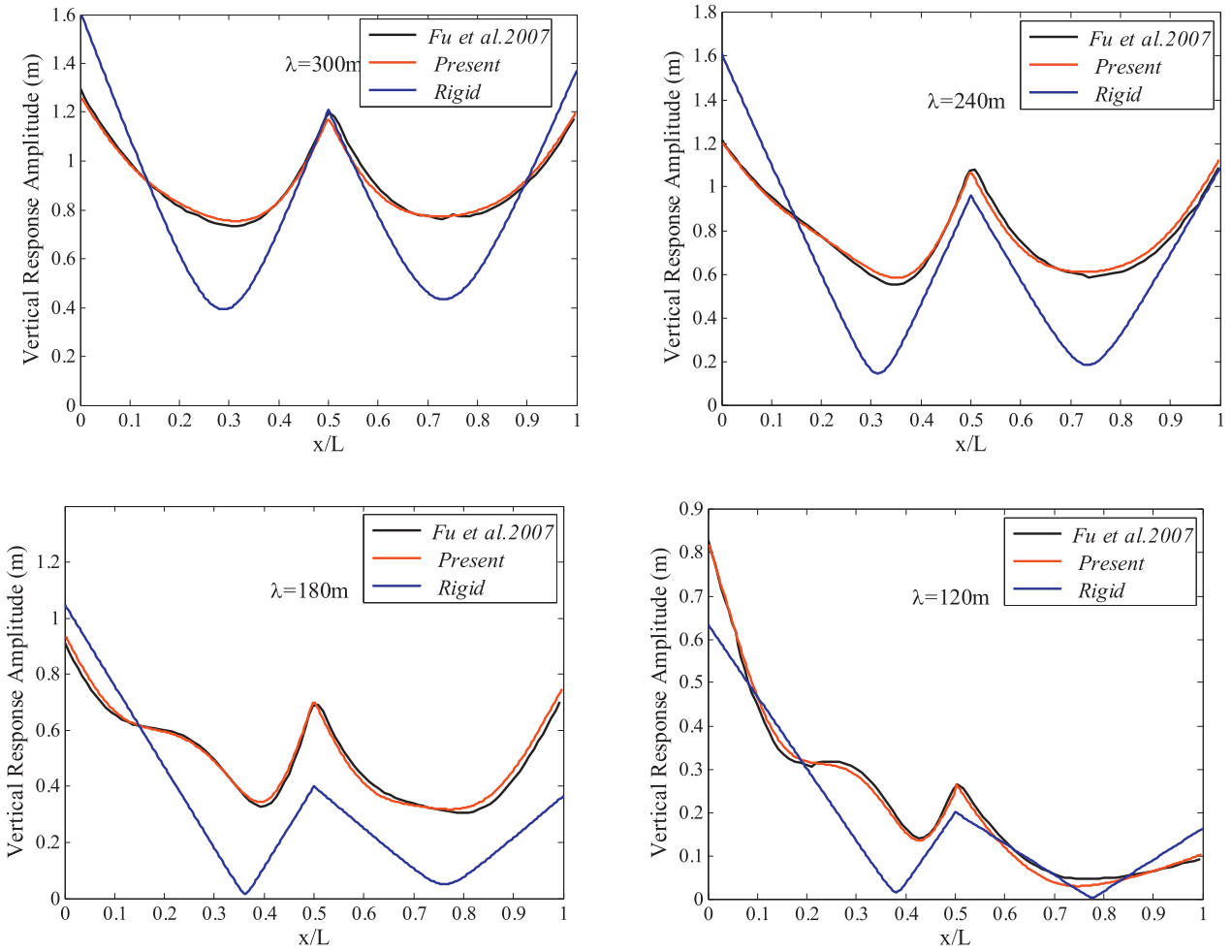

Fig. 8. Vertical response amplitude of the longitudinal centerline with a hinged connector.

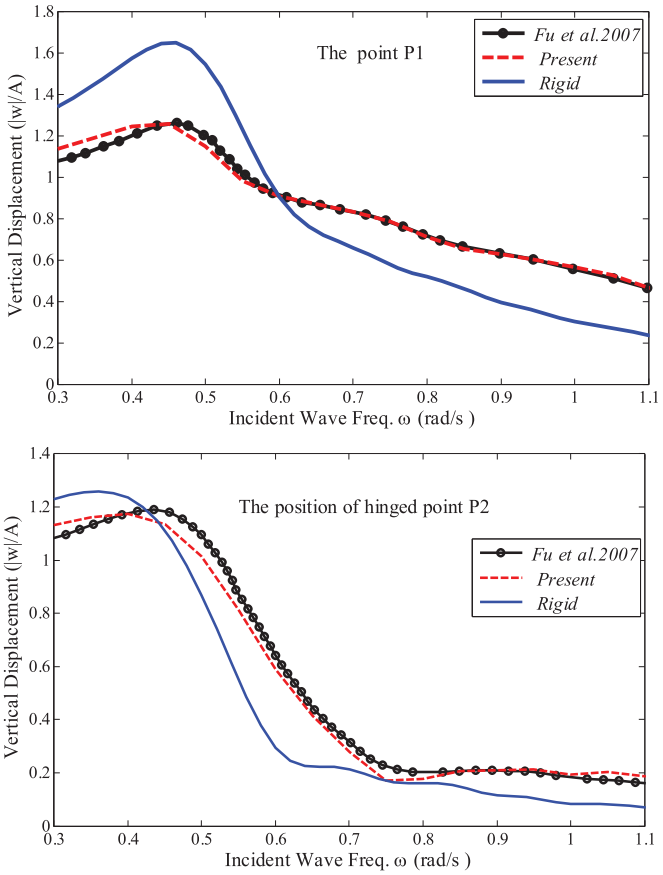

Fig. 9. Vertical response of the model at points P_1 and P_2.

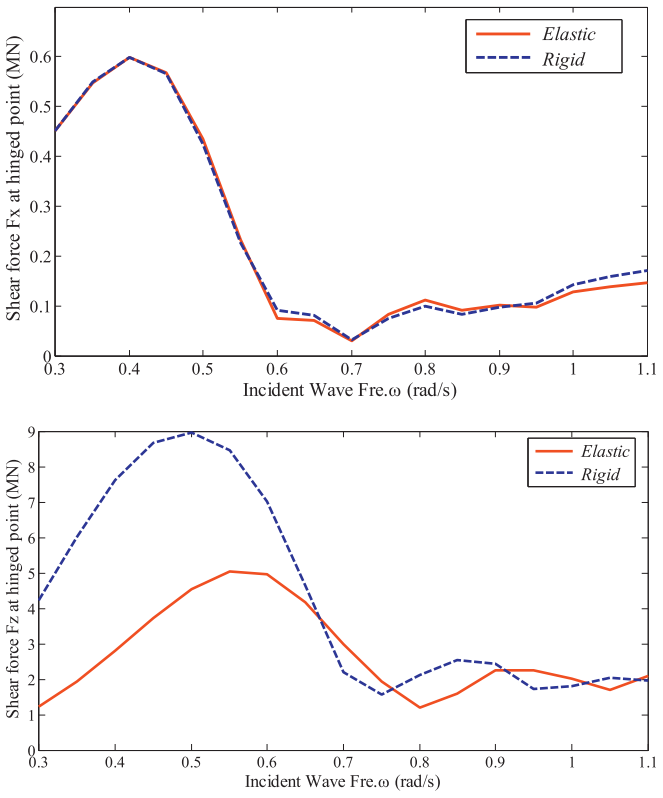

Fig. 10. Shear force F_z and F_x at the hinged point.

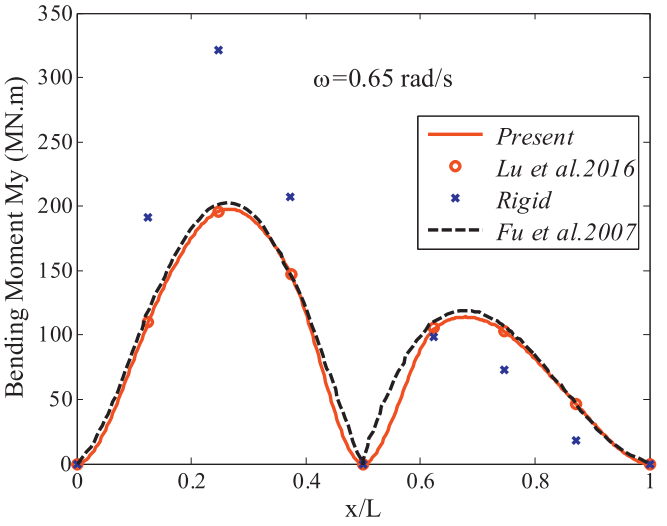

Fig. 11. Bending moment amplitude distributions along the length of the hinged structure.

the approach proposed by Lu et al. (2016) and Fu et al. (2007). Also significant differences are found for the rigid and flexible structure. For the present approach, it is convenient to consider the effects of structural stiffness on the dynamic response of the hinged multi-module VLFS. The change of structural stiffness will only affect the stiffness matrix in the hydroelastic equation of flexible structure (see Eqs. (10) and (15)), which means that the distribution of moment along the VLFS can be easily and quickly calculated for different structural stiffness (for traditional hydroelasticity theory, mode analysis is needed for every time of the change of structural stiffness). The bending moment of the hinged rigid body is obtained by choosing a very large value Young's modulus.

As shown in Table 1, the Young's modulus has been assumed to be $E = 1.19 \times 10^{10}$ N/m^2. The change of the Young's modulus is from $0.1E$ to $10E$. The hinged structure's

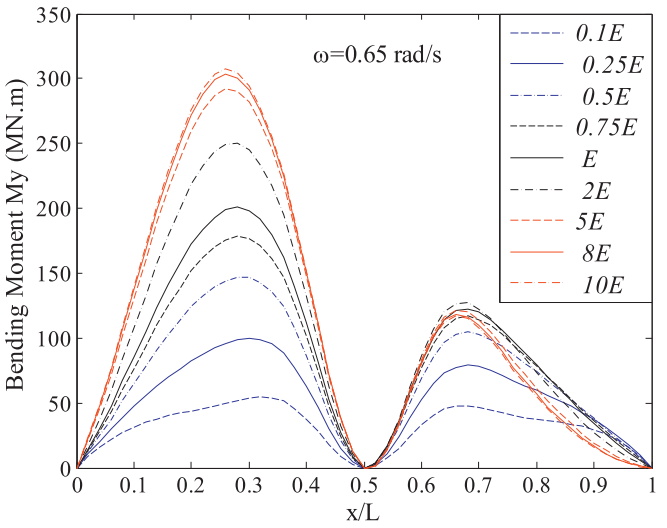

Fig. 12. Bending moment for different values of the Young's modulus.

bending moment is shown in Fig. 12 under the influence of different values of the Young's modulus. It can be clearly seen that, for the first module, the bending moment increases with increasing stiffness. For the second module, the bending moment first increases and then decreases with increasing stiffness. The maximum bending moment of the first module is, however, always greater than that of the second.

4. Conclusions

This paper presents a new method to calculate the hydroelastic response of hinged VLFSs. A hinged two-module flexible structure is used to confirm the present approach. For each module, the hydroelasticity theory proposed by Lu et al. (2016) is adopted to consider the coupled effects of wave dynamics and structural deformation. The continuous condition at the connection position between two adjacent modules is also satisfied. The results calculated by the present new method are compared with those obtained using three-dimensional hydroelasticity theory (Fu et al., 2007), which shows rather good agreement. For comparison, the hinged two-module rigid structure is also investigated, and results show that the elasticity of the structure has a great influence on the bending moment, as well as the dynamic response of the flexible structure. As demonstrated by the calculations presented in this paper, the new method has many applications, including dealing with complex structures consisting of different modules (rigid or elastic) and different forms of connectors.

Appendix.

The stiffness matrix $[K]_{i-j}$ in Eq. (12):

$$
[\mathrm{K}]=\begin{bmatrix}
\frac{EA}{l} & & & & & & & & & & & \\
0 & \frac{12EI_z}{l^3(1+\beta_y)} & & & & & S & y & m & m & & \\
0 & 0 & \frac{12EI_y}{l^3(1+\beta_z)} & & & & & e & t & r & & \\
0 & 0 & 0 & \frac{G\kappa h^3 b}{l} & & & & & y & & & \\
0 & 0 & \frac{-6EI_y}{l^2(1+\beta_z)} & 0 & \frac{(4+\beta_z)EI_y}{l(1+\beta_z)} & & & & & & & \\
0 & \frac{6EI_z}{l^2(1+\beta_y)} & 0 & 0 & 0 & \frac{(4+\beta_y)EI_z}{l(1+\beta_y)} & & & & & & \\
-\frac{EA}{l} & 0 & 0 & 0 & 0 & 0 & \frac{EA}{l} & & & & & \\
0 & \frac{-12EI_z}{l^3(1+\beta_y)} & 0 & 0 & 0 & \frac{-6EI_z}{l^2(1+\beta_y)} & 0 & \frac{12EI_z}{l^3(1+\beta_y)} & & & & \\
0 & 0 & \frac{-12EI_y}{l^3(1+\beta_z)} & 0 & \frac{6EI_y}{l^2(1+\beta_z)} & 0 & 0 & 0 & \frac{12EI_y}{l^3(1+\beta_z)} & & & \\
0 & 0 & 0 & \frac{-G\kappa h^3 b}{l} & 0 & 0 & 0 & 0 & 0 & \frac{G\kappa h^3 b}{l} & & \\
0 & 0 & \frac{-6EI_y}{l^2(1+\beta_z)} & 0 & \frac{(2-\beta_z)EI_y}{l(1+\beta_z)} & 0 & 0 & 0 & \frac{6EI_y}{l^2(1+\beta_z)} & 0 & \frac{(4+\beta_z)EI_y}{l(1+\beta_z)} & \\
0 & \frac{6EI_z}{l^2(1+\beta_y)} & 0 & 0 & 0 & \frac{(2-\beta_y)EI_z}{l(1+\beta_y)} & 0 & \frac{-6EI_z}{l^2(1+\beta_y)} & 0 & 0 & 0 & \frac{(4+\beta_y)EI_z}{l(1+\beta_y)}
\end{bmatrix}
$$

The size of the symmetric matrix is 12 × 12. The matrix is affected by the size of each submodule, Young modulus and Poisson ratio. l is the length of beam element (the dimension along x axis). b is the dimension along y axis. h is the dimension along z axis. κ is a constant related to b and h. A is cross-sectional area. E is Young modulus. β_y is the correction factor considering shear deformation for the beam element bending in xoy plane. β_z is the correction factor considering shear deformation for the beam element bending in xoz plane. I_y is the moment of inertia around the y axis. I_z is the moment of inertia around the z axis. G is shear modulus.

References

Fu, S., Moan, T., Chen, X., Cui, W., 2007. Hydroelastic analysis of flexible floating interconnected structures. Ocean Eng. 34 (11), 1516–1531.

Gao, R.P., Tay, Z.Y., Wang, C.M., Koh, C.G., 2011. Hydroelastic response of very large floating structure with a flexible line connection. Ocean Eng. 38 (17), 1957–1966.

Gou, Y., Teng, B., Ning, D.Z., 2004. Interaction effects between wave and two connected floating bodies. Eng. Sci. 6 (7), 75–80.

Kim, B.W., Hong, S.Y., Kyoung, J.H., Cho, S.K., 2007. Evaluation of bending moments and shear forces at unit connections of very large floating structures using hydroelastic and rigid body analyses. Ocean Eng. 34 (11), 1668–1679.

Li, Q.Y., Wang, N.C., Yi, D.Y., 1986. Numerical Analysis. Hua Zhong University of Science Press (In Chinese).

Lu, D., Fu, S., Zhang, X., Guo, F., Gao, Y., 2016. A method to estimate the hydroelastic behaviour of VLFS based on multi-rigid-body dynamics and beam bending. Ships Offshore Struct. 1–9.

McGuire, W., Gallagher, R.H., Ziemian, R.D., 2000. Matrix Structural Analysis, second ed. Faculty Books, p. 7.

Newman, J.N., 1994. Wave effects on deformable bodies. Appl. Ocean Res. 16 (1), 47–59.

Pan, Y., Sahoo, P.K., Lu, L., 2016. Numerical study of hydrodynamic response of mooring lines for large floating structure in South China Sea. Ships Offshore Struct. 11 (7), 774–781.

Riyansyah, M., Wang, C.M., Choo, Y.S., 2010. Connection design for two-floating beam system for minimum hydroelastic response. Mar. Struct. 23 (1), 67–87.

Tsubogo, T., Okada, H., 1998. An estimation method of dynamic behavior of huge mat-type floating structures using simple beam modeling. In: American Society of Mechanical Engineers, 17th International Conference on Offshore Mechanics and Arctic Engineering (USA), p. 8.

Tuitman, J.T., Malenica, Š., Van'T Veer, R., 2012. Generalized modes in time-domain seakeeping calculations. J. Ship Res. 56 (4), 215–233.

Wu, Y.S., 1984. Hydroelasticity of Floating Bodies. Brunel University, UK (Ph.D. Thesis).

Wu, H.L., Chen, X.J., Huang, Y.X., Wang, B., 2014. Influence of the legs underwater on the hydrodynamic response of the multi-leg floating structure. Ships Offshore Struct. 9 (6), 578–595.

Yago, K., Endo, H., 1996. On the hydroelastic response of box-shaped floating structure with shallow draft. J. Soc. Naval Archit. Jpn. 180, 341–352.